Effect of Isotacticity on Formation of Mesomorphic Phase of Isotactic Polypropylene

Takashi Konishi, Koji Nishida,* Toshiji Kanaya, and Keisuke Kaji

Institute for Chemical Research, Kyoto University, Uji, Kyoto-fu 611-0011, Japan

Received April 30, 2005; Revised Manuscript Received July 28, 2005

ABSTRACT: The effect of isotacticity on the mesomorphic phase-forming properties of isotactic polypropylene (iPP) is reported. Only iPP having high isotacticity (iPP-HT) can form the mesomorphic phase by a rapid quench, but iPP having low isotacticity (iPP-LT) cannot form the mesomorphic phase though it crystallizes by the same quenching rate. These results suggest that the mesomorphic phase of iPP is closely related to the stereoregularity of the polymer chain. The mesomorphic phase in the iPP-HT shows longer regular 3/1 helices than in the crystalline iPP-LT. The structure and formation mechanism of the mesomorphic iPP are considered analogous to those of liquid crystals since the average length of the long regular 3/1 helices in the mesomorphic iPP acting as rodlike segments is sufficiently large to fulfill a criterion for the formation of liquid crystalline phase. From this criterion, the minimum requirement of isotacticity to form the mesomorphic phase is also estimated.

1. Introduction

Three kinds of crystalline modifications of isotactic polypropylene (iPP) have so far been known as α (monoclinic), β (hexagonal), and γ (orthorhombic) forms.[1−4] The crystalline structures of these forms are specified by four types of 3/1 helices, i.e., the combination of left- and right-handed helices and up and down stems concerning the CH_3 group.[4] Although the α form is readily obtained, special nucleating reagent is required for the formation of the β form,[5] and also specific thermal conditions[6,7] or high pressure[8] is often required for the formation of the γ form.

Meanwhile, it is well-known that the molten iPP transforms into the so-called mesomorphic phase when it is quenched below 0 °C with a rate faster than 80 °C/s.[9] The structure of the mesomorphic phase is still an open question. Some researchers assign the structure to the smectic phase.[1,10] Other explanations are based on defects of crystal: paracrystalline,[11,12] conformational disorder (condis) crystal,[13] and micro- or nanocrystal.[14,15] The common understanding on the structure of the mesomorphic phase is limited as below. The mesomorphic phase has local order as was revealed by wide-angle X-ray diffraction (WAXD) measurements.[1,12] According to Fourier transform infrared spectroscopy (FT-IR), the conformation of the mesomorphic phase is 3/1 helix as well as that of the crystalline structures mentioned above; however, the sense of the helix (left- and right-handed) has no particular rule.[16] On the nanoscopic scale, the morphology of the mesomorphic iPP is characterized by the so-called "nodule" of polygonal or spherical shape as was examined by transmission electron microscopy (TEM).[10,17,18] The diameter of the nodule is ca. 10 nm at room temperature. This value is also confirmed by small-angle X-ray scattering (SAXS) measurements.[10]

The mesomorphic iPP can also be formed from an ultraquenched glassy state.[19] With increasing the temperature of the glassy iPP from ca. −30 °C, the broad double peaks being characteristic of the mesomorphic iPP gradually appear in WAXD. When the temperature exceeds 40−80 °C, the mesomorphic iPP starts to transform into the α form.[20,21] Thus, the mesomorphic phase of iPP has some intermediate structure between glass and crystal. The formation mechanism of the mesomorphic phase is far less understood than the structure.

In this study, we will examine the condition for the formation of the mesomorphic phase, especially from the viewpoint of tacticity. Providing that the defects of crystal are closely related to the formation of the mesomorphic phase, lowering of the tacticity should enhance the formation of the mesomorphic phase. On the other hand, if the mesomorphic phase is liquid-crystal-like, mesogenic segments are required. Regular helical conformation plays the role of a mesogenic segment.[22−25] For the formation of the regular helical conformation, higher tacticity is essential. To characterize iPP samples with different degrees of isotacticity, FT-IR, WAXD, and SAXS have been used, which are useful techniques to estimate the length of the regular helical conformation, to distinguish the mesomorphic phase from the crystalline and amorphous states, and to estimate long spacing, respectively.

2. Experimental Section

Two kinds of iPP having different degrees of isotacticity and an atactic polypropylene (aPP) were used as obtained in this study. A high isotacticity polymer (iPP-HT) having a degree of isotacticity (meso pentad: *mmmm*) of 0.982, a weight-average molecular weight $M_w = 208\,000$, and a polydispersity of $M_w/M_n = 5.47$ was supplied from Mitsui Chemical Co. Ltd. A low isotacticity polymer (iPP-LT) having a degree of isotacticity (*mmmm*) of 0.482, $M_w = 222\,000$, and $M_w/M_n = 1.86$ was supplied from Idemitsu Kosan Co. Ltd. As an atactic polymer (aPP), a sample having a degree of isotacticity (meso tetrad: *mmm*) of 0.125, $M_w = 118\,000$, and $M_w/M_n = 1.27$ was used.[26]

The iPP-HT that was melted at 220 °C for 5 min on a hot-stage and then crystallized at 130 °C for 1 h on another hot-stage is designated sample A. The iPP-HT, iPP-LT, and aPP that were melted at 220 °C on the hot-stage and then quenched to 0 °C by dipping into ice water are designated sample B, sample C, and sample D, respectively. The quenching was

* Corresponding author: e-mail knishida@scl.kyoto-u.ac.jp; tel +81-774-38-3141; fax +81-774-38-3146.

10.1021/ma050908f CCC: $30.25
Published on Web 09/16/2005

Table 1. Materials and Thermal Treatments

sample	material	thermal treatment
A	iPP-HT	200 °C (melt) → 130 °C (1 h) → rt
B	iPP-HT	200 °C (melt) → 0 °C → rt
C	iPP-LT	200 °C (melt) → 0 °C → rt
D	aPP	200 °C (melt) → 0 °C → rt

Table 2. Results of Component Analysis by WAXD

sample	crystalline (α, γ)[a] (%)	mesomorphic (%)	amorphous (%)
A	79 (54, 26)		21
B		54	46
C	29 (25, 4)		71
D			100

[a] The figures in parentheses (α, γ) indicate crystallinity indices for α and γ components, respectively.

made fast enough to fulfill the critical rate 80 °C/s; the temperature of the quenched sample was checked with a thermocouple detector whose thin thermoelement was buried in the sample film.[27] These thermal treatments are listed in Table 1. Sample films 100 μm thick were used for FT-IR measurements. For WAXD and SAXS measurements, five pieces of sample film 200 μm thick were piled to enhance the scattering intensities. WAXD, FT-IR, and SAXS measurements for these four PP samples were carried out at room temperature using a Rigaku Denki RINT-2200 diffractometer, a Nicolet Impact 410 system, and the beamline BL-10C in the Photon Factory at National Laboratory for High Energy Physics, Tsukuba, Japan, respectively. The SAXS covered a range of 6.0×10^{-3}–1.8×10^{-1} Å^{-1} in scattering vector q (= $4\pi \sin\theta/\lambda$; λ and 2θ being X-ray wavelength and scattering angle, respectively).

3. Results

3.1. WAXD Measurements. Parts a–d of Figure 1 display WAXD profiles for samples A–D, respectively. Component analysis for these WAXD profiles was carried out, assuming each profile consists of α-crystalline, γ-crystalline,[28] mesomorphic, and amorphous fractions. Fitting curves and their constituents are also displayed in Figure 1a–d. Sample A shows sharp α-crystalline Bragg peaks at 2θ = 14.1°, 16.9°, 18.6°, 21.6°, and 21.9°.[1,12] Most of these α-crystalline peaks overlap γ-crystalline peaks, but they are very weak and difficult to see; nevertheless, a weak broad peak specific to γ-crystalline is actually observed at 2θ = 20°.[7] Sample B shows two broad peaks at around 2θ = 15 and 21°, which are known as characteristic features of mesomorphic phase of iPP.[1,12] Sample C shows α-crystalline peaks and a faint γ-crystalline peak. Sample D shows only an amorphous halo at around 16°. The crystallinity index of sample A obtained by the component analysis was 79%, and the rest was amorphous. The component of mesomorphic phase in sample B was 54%, and the rest was amorphous. The crystallinity index of sample C was 29%, and the rest was amorphous. No significant fraction of mesomorphic phase was detected for sample C, although sample C was quenched as rapidly as sample B. Results of these component analyses are listed in Table 2. The figures in parentheses (α, γ) show α- and γ-crystallinity indices, respectively.

Here it should be noted that the fraction of the γ-phase is affected by the crystallization temperature and the distribution of pentads other than *mmmm* pentad[6] as well as by the cooling rate.[7] The latter literature showed that the fraction of γ-phase decreases with increasing the cooling rate, whereas the fraction of α-phase increases. The quenching speed applied to samples B and C in this study is far faster (>80 °C/s = 4800 °C/min) than the cooling rates scanned in the latter literature (0.5–50 °C/min). The quenched iPP-HT (sample B) does not show any fraction of γ-phase. This result is consistent with the result of the latter literature. In such a rapid quench, the competition between α-phase and mesomorphic phases becomes leading. On the other hand, the quenched iPP-LT (sample C) shows a small fraction of γ-phase, although the quenching rate was the same rate as that of the sample B. This result is also qualitatively consistent with the result of the latter literature. The latter literature also showed that the relative fraction of γ-phase of the lower tacticity iPP is larger than that of the higher tacticity, and the fraction of γ-phase also decreases with increasing the cooling rate, but it tends to remain in rather high cooling rate.

It was reported that crystalline polymers with higher tacticity usually showed higher crystallinity when the same thermal treatment was applied.[29] However, this is not always valid, but it depends on the crystallization conditions. Thus, sample C with low tacticity (iPP-LT) shows some crystallinity index, but sample B (iPP-HT) has no crystallinity index despite its higher tacticity. The rapid quenching hinders the crystallization of the higher tacticity polymer rather than the lower tacticity polymer. In other words, the mesomorphic phase of iPP is not related to the defects of crystal due to stereoirregularity, since the decrease of tacticity does not enhance the formation of the mesomorphic phase.

3.2. FT-IR Measurements. In FT-IR spectra, some absorption bands are sensitive to the physical state and conformation as well as primary chemical structure of polymers. For iPP, these bands have been classified into crystal/amorphous bands, helical bands, and tacticity bands.[30] The 3/1 helical conformation bands of iPP appear at 1330, 1303, 1220, 1167, 1100, 998, 940, 900, 841, and 808 cm^{-1}.[30] The isotactic band appears at 973 cm^{-1}.[30] The syndiotactic band appears at 963 cm^{-1}.[31] The amorphous band appears at 1156 cm^{-1}.[30] The isotactic band and the 3/1 helical conformation bands are related to the critical lengths of regular isotactic sequence. The critical length is defined as a minimum number (m) of isotactic monomer units being sufficient for the appearance of those bands. The absorption bands at 973, 998, 841, and 1220 cm^{-1} have so far been assigned to m = 3–4,[30] 10,[30,32] 12,[30,33,34] and 14 or more,[35,36] respectively. It should be noted that these bands will appear in not only the crystalline phase but also mesomorphic and amorphous phases, when the conditions mentioned above are fulfilled.

Figure 2 shows the FT-IR spectra of samples A–D. For the quantitative discussion later on, the absorption bands at around 841, 963, 973, 998, and 1220 cm^{-1} for each sample were fitted to Lorentzian function, and the obtained absorbancies A_{841}, A_{963}, A_{973}, A_{998}, and A_{1220} for these bands, respectively, are listed in Table 3. Comparison of the spectra between samples B and C concerning the band at 1220 cm^{-1} ($m \geq 14$) is especially interesting. Sample B shows this long helical conformation band; however, sample C does not show such a band. This fact indicates that the crystalline phase of the quenched iPP-LT consists of shorter helical segments than the mesomorphic phase of the quenched iPP-HT. Considering the results of FT-IR together with WAXD, a specific kinetic path to the mesomorphic phase seems to be opened when the isotacticity is high enough and the regular helical segment is long enough.

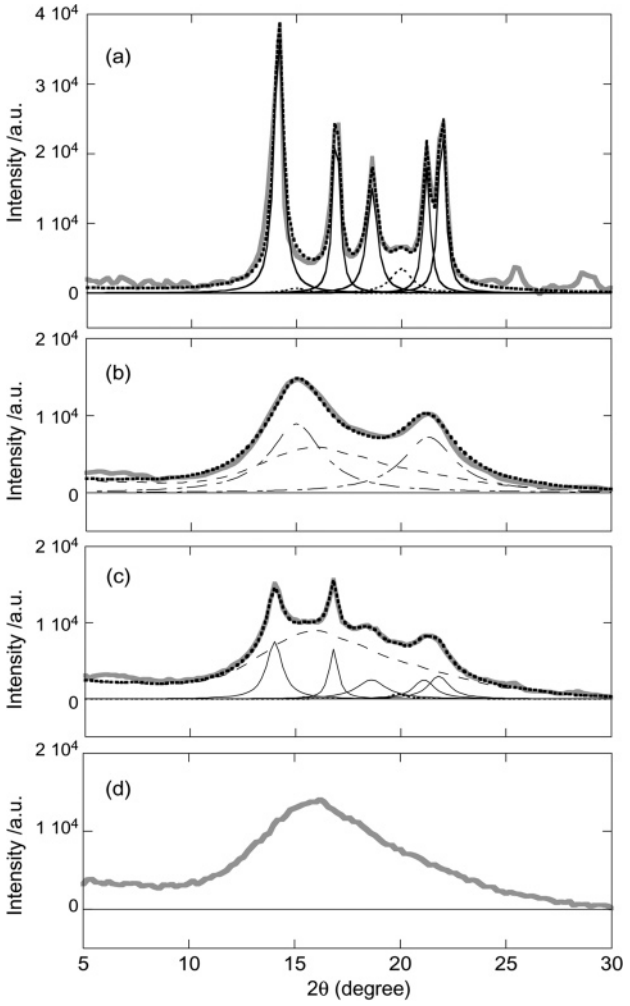

Figure 1. WAXD profiles of samples A−D in (a)−(d), respectively. Observed (thick gray lines) and fitting (thick dotted lines) curve reproduced by summing up the constituents separated by the component analysis where α-crystalline form (thin solid lines), γ-crystalline form (thin dotted lines), mesomorphic phase (thin chain lines), and amorphous phase (thin broken lines).

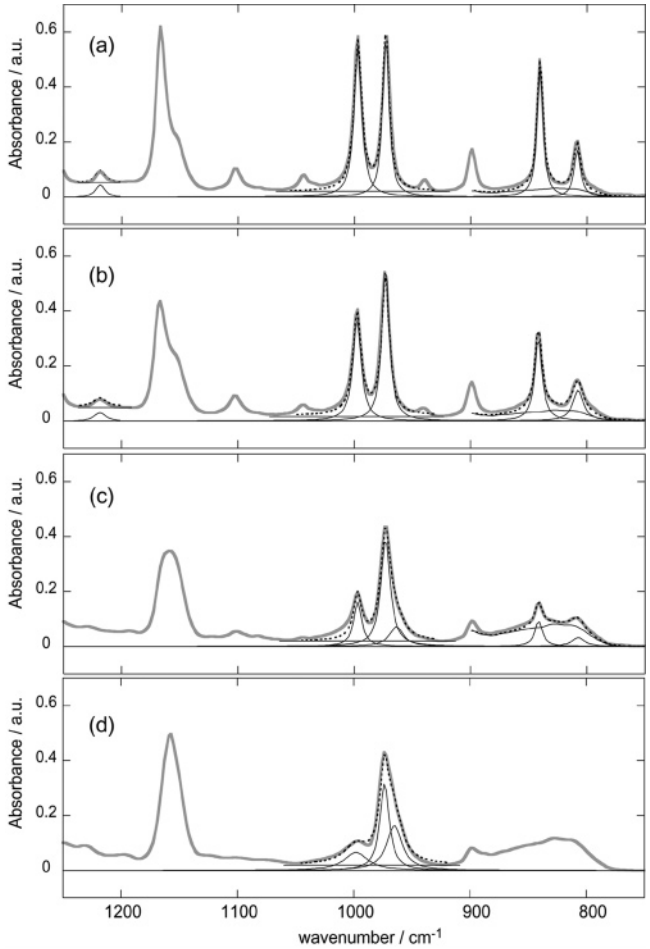

Figure 2. FT-IR spectra of samples A−D in (a)−(d), respectively. Observed (thick solid lines) and fitting (thin dotted lines) component curves with Lorenzian function and the sum of fitting component curves (dotted lines).

3.3. SAXS Measurements. Figure 3 shows the SAXS profiles of samples A−D. Samples A−C show a broad peak at q = 0.03, 0.065, and 0.056 Å^{-1}, respectively. Sample D shows no peaks. SAXS peaks for crystalline polymers are usually assigned to an interlamellar correlation or the so-called long period. However, the SAXS peak at q = 0.065 Å^{-1} for the mesomorphic iPP cannot be assigned to the interlamellar correlation. It should be interpreted as an internodule correlation since the electron micrograph for the mesomorphic iPP shows densely packed spherical or polygonal objects, i.e., the so-called nodules.[17,18] The internodule correlation observed in TEM indeed corresponds to a distance calculated from peak position in SAXS curve.[10,20] Hence, we assign the peaks of crystalline samples A and C to the interlamellar correlation while that of sample B to the internodule correlation. The obtained SAXS profiles for samples A and C are transformed into one-dimensional electron density correlation factor $K(z)$, and the values of lamellar thickness are extracted from $K(z)$ according to Strobl's method:[37]

$$K(z) = \frac{1}{r_e}\frac{1}{(2\pi)^3}\int_0^\infty \cos(qz)4\pi q^2 I(q)\,dz \qquad (1)$$

where r_e and z are classical electron radius and distance in the real space. Figure 4 shows $K(z)$ vs z plots for samples A and C. Here it should be noted that the so-called "self-correlation triangle" of $K(z)$ reflects the electron density correlation within an interlamellar region or within a lamella, depending on whether the degree of crystallinity is more or less than 50%, which is well-known as the Babinet principle. Since the degrees of crystallinity for samples A and C determined by WAXD are 79% and 29%, respectively, the triangles for samples A and C correspond to the correlation within an interlamellar region and within a lamella, respectively. The obtained lamellar thickness and long period of sample A are therefore 137 Å (= 193 Å − 56 Å) and 193 Å, respectively. Likewise, those of sample C are 28 and 98 Å, respectively. Dividing the lamellar thickness by the long period, the crystallinity indices were roughly calculated from these values. The obtained crystallinity indices of sample A and C are 71% and 29%, respectively, which correspond well to those obtained by the WAXD analysis (see Table 2). Because the projected length of one monomer unit on the axis of 3/1 helix of iPP is 2.17 Å,[31,38] the obtained lamellar thickness 28 Å of the sample C corresponds to 13 monomer units in a helical sequence. This number of monomer units is consistent with the results of FT-IR; sample C did not show the 1220 cm^{-1} band ($m \geq 14$). The average domain size of a nodule is considered to be equivalent to or somewhat less than the internodule distance of 96.7 Å

Table 3. FT-IR Absorbance for Characteristic Bands

sample	A_{841} ($m = 12$)	A_{963} (syndio)	A_{973} ($m = 3-4$)	A_{998} ($m = 10$)	A_{1220} ($m \geq 14$)	A_{973}/A_{973A}
A	0.469		0.548	0.545	0.0424	1
B	0.293		0.537	0.365	0.0288	0.980
C	0.0890	0.0722	0.395	0.167		0.720
D		0.163	0.314	0.0665		0.573

calculated from the peak position in the SAXS curve ($= 2\pi/0.065$). The size is long enough to contain the long helical segments ($m \geq 14$).

4. Discussion

In this study we have examined the mesomorphic phase-forming properties of iPP having three different degrees of isotacticity. As the results, iPP-HT ($mmmm = 0.982$) could form the mesomorphic phase; however, iPP-LT ($mmmm = 0.482$) could not form the mesomorphic phase. In this section, we will discuss the minimum requirements of isotacticity for the formation of the mesomorphic phase, from the standpoint of the liquid crystal formation mechanism.

4.1. Estimation of Isotactic Sequence Lengths. First, we will derive mathematical expressions for the average number of monomer units in an isotactic block sequence, $\langle n \rangle_{iso}$, starting from Kissin's treatment.[30] The value of $\langle n \rangle_{iso}$ will be estimated from the data of NMR and FT-IR. Assuming that isotactic block sequences in a long polymer chain ($\gg n$) consist of n monomer units, the number of their isotactic linkages is $n - 1$ and both their ends have syndiotactic linkage. Then, the fraction of monomer units constituting such isotactic blocks is given by[30]

$$\delta_n = np^{n-1}(1-p)^2 \quad (n = 1, 2, 3, ...) \tag{2}$$

where p is the probability of isotactic addition. Note that $1 - p$ is the probability of syndiotactic addition, and the case $n = 1$ for eq 2 means syndiotactic addition. Accordingly, the sum of δ_n from $n = 1$ to ∞ is normalized to unity ($\sum_{n=1}^{\infty}\delta_n = 1$). The total fraction of monomer units belonging to the sequences having more than $n - 1$ isotactic linkages is also given by[30]

$$\chi_n = \sum_{k=n}^{\infty}\delta_k = (n - np + p)p^{n-1} \tag{3}$$

Assuming that the total number of monomer units in a long polymer chain is N, the sum of monomer units constituting the isotactic blocks of n monomer units is given by $N\delta_n$, and the number of such isotactic blocks in the long polymer chain is given by $N\delta_n/n$. The total number of blocks is $N\sum_{n=1}^{\infty}\delta_n/n$. Then, the average number of monomer units, $\langle n \rangle_{iso}$, in one isotactic block is derived as follows:

$$\langle n \rangle_{iso} = N/[N\sum_{n=1}^{\infty}\delta_n/n] = (1-p)^{-1} \tag{4}$$

As was mentioned in Experimental Section, meso pentad values of iPP-HT and iPP-LT and a meso tetrad value of aPP obtained by NMR are 0.982, 0.482, and 0.125, respectively. Accordingly, the probabilities of isotactic addition, p's, for iPP-HT, iPP-LT, and aPP are $0.982^{1/4} = 0.996$, $0.482^{1/4} = 0.833$, and $0.125^{1/3} = 0.5$, respectively. Substituting 0.996 for p and 3, 4 for n in eq 3, χ_{3-4} for sample A is estimated to be 0.99995−0.99990. This value is almost unity. As was mentioned in the section of FT-IR, the absorbance A_{973} is assigned to $m = 3-4$. Therefore, the values A_{973C} and A_{973D} relative to A_{973A} should correspond to χ_{3-4} for the samples C and D, respectively. Because of $A_{973C}/A_{973A} = 0.720$ and $A_{973D}/A_{973A} = 0.573$, p's of iPP-LT and aPP are calculated as 0.651−0.740 and 0.549−0.656, respectively. Substituting these values for p in eq 4, $\langle n \rangle_{iso}$ of iPP-LT and aPP are calculated to be 2.87−3.85 and 2.22−2.91, respectively. On the other hand, substituting the probabilities of isotactic addition obtained by NMR directly for p in eq 4, $\langle n \rangle_{iso}$ of iPP-HT, iPP-LT, and aPP are calculated to be 250, 5.99, and 2.00, respectively. Table 4 summarizes the average numbers of monomer units in one isotactic block, $\langle n \rangle_{iso}$, obtained by FT-IR and NMR results. Here, it should be noted that the average number of monomers, 250, in one isotactic block se-

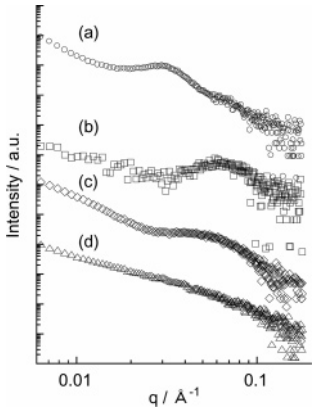

Figure 3. SAXS profiles of samples A−D in (a)−(d), respectively.

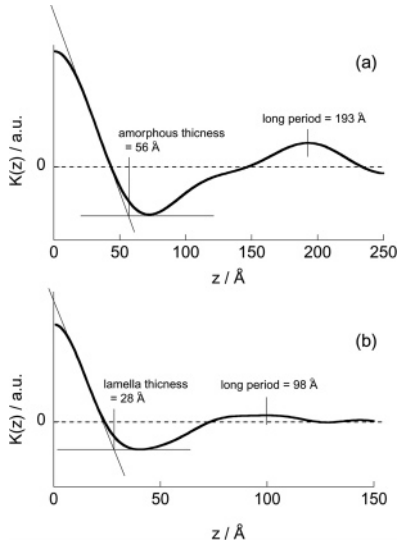

Figure 4. $K(z)$ vs z plots of sample A (a) and C (b) from SAXS profiles of Figure 3. The "self-correlation triangles" of $K(z)$ for samples A (a) and C (b) correspond to the correlation within an interlamellar region and within a lamella, respectively.

Table 4. Average Number of Monomer Units $\langle n \rangle_{iso}$ per One Isotactic Block

sample	iPP-HT	iPP-LT	aPP
$\langle n \rangle_{iso}$ (FT-IR)		2.87−3.85	2.22−2.91
$\langle n \rangle_{iso}$ (NMR)	250	5.99	2.00

quence for iPP-HT is considerably large compared with the internodular distance of 96.7 Å obtained by SAXS. This probably means that the isotactic sequences are folded in the nodule particle; in other words, it means that all monomers in the isotactic block sequence do not transform continuously into 3/1 helix.

4.2. Critical Length of Rodlike Segments for the Mesomorphic Phase. Next, we will derive the critical length of rodlike segment for the formation of liquid crystalline phase. Then, assuming the block of regular 3/1 helices of iPP as the rodlike segment,[39] we will estimate the minimum requirement for $\langle n \rangle_{iso}$ to form such a block of regular 3/1 helices. Doi and co-workers[40] have theoretically investigated the formation mechanism of lyotropic liquid crystal in a stiff polymer system using two order parameters of concentration and orientation. This theory predicts that isotropic-to-nematic (I−N) phase transition occurs by the excluded-volume effect of rodlike segments when a concentration of rodlike segments exceeds a critical concentration. This critical concentration ν^* is given by

$$\nu^* = 4.19/(bL^2) \tag{5}$$

where b and L is a diameter and the length of the rod polymer. Kaji and co-workers applied Doi's theory to describe the preparatory mechanism of polymer crystallization.[22−25] As described above, they assumed that regular helical sequences in real polymer chains are the rodlike segments of liquid crystalline polymer and calculated the concentration ν of regular helical segments as follows:

$$\nu = \rho N_A/[(L/l_0)M_0] \tag{6}$$

where ρ, N_A, L, l_0, and M_0 are the density of the polymer, Avogadro's number, the average length of helical segments, the projected length of a monomer to the axis of helix, and molecular weight of the monomer, respectively. From eqs 5 and 6, the critical length L_c of helical segments for the I−N phase transition is given by[25]

$$L_c = 4.19M_0/(bl_0\rho N_A) \tag{7}$$

Numerical parameters M_0, b, l_0, and ρ for iPP are 42 g/mol, 6.65 Å, 2.17 Å, and 0.85 g/cm^3, respectively.[31,38] These values yield L_c = 23.8 Å, which corresponds to 10.96 or about 11 monomer units.[38] This value is the minimum requirement for $\langle n \rangle_{iso}$.

4.3. Why Does Only iPP-HT Assume the Mesomorphic Phase? As is listed in Table 4, the estimated values of $\langle n \rangle_{iso}$ = 2.87−3.85 (FT-IR) or 5.99 (NMR) for iPP-LT are considerably less than the critical value of 11 though there is some difference between NMR and FT-IR. Therefore, iPP-LT cannot assume the nematic phase. In contrast, $\langle n \rangle_{iso}$ for iPP-HT is 250, which is much larger than the critical value and so meets the requirement for the I−N phase transition. These arguments are consistent with the present experimental results of WAXD; the quenched iPP-HT showed the characteristic features of the mesomorphic phase and the quenched iPP-LT did not (see Figure 1 and Table 2). By substituting the value of 10.96 for $\langle n \rangle_{iso}$ in eq 4, we obtain 0.908 as the critical probability p^* of isotactic addition required for the formation of the mesomorphic phase, which corresponds to *mmmm* = 0.680. As a matter of course, the critical value p^* is lower than that of iPP-HT and higher than that of iPP-LT.

5. Conclusion

We have examined the mesomorphic phase-forming properties for iPP with three different degrees of isotacticity. As the results of WAXD, iPP having higher isotacticity (*mmmm* = 0.982) formed the mesomorphic phase, however, iPP having lower isotacticity (*mmmm* = 0.482) did not form the mesomorphic phase but the α-crystalline form. In FT-IR spectra, the mesomorphic iPP-HT showed a long helix ($m \geq 14$) band at 1220 cm^{-1}; however, the crystalline iPP-LT did not show the band. Analysis of SAXS showed that the crystalline iPP-LT consists of lamellar structure having its thickness of 13 monomer units and the mesomorphic iPP consists of noduler structure having a diameter corresponding to more than 14 monomer units. The present experimental results indicate that the mesomorphic iPP-HT consists of regular 3/1 helices longer than the crystalline iPP-LT. The formation mechanism of the mesomorphic phase of iPP could be explained reasonably by Doi's theory for polymer liquid crystals.[22−25,40] Therefore, it is strongly suggested that the mesomorphic phase is not a highly defected crystal but a liquid-crystal-like structure. Assuming the block of regular 3/1 helices of iPP as the rodlike segment, we estimated the critical probability p^* of isotactic addition required for the formation of the mesomorphic phase and the critical pentad (*mmmm*)*, finding 0.908 and 0.680, respectively. To our knowledge, both the experimental and theoretical estimation of such critical values for the formation of the mesomorphic phase of iPP have not been reported. In this study, we have not examined the effect of stereodefect distributions. It could be interesting if the mesomorphic phase-forming properties are compared among samples having the same or similar degree of *mmmm* pentad but having different distribution in other pentads, as was successfully studied for the γ-phase formation.[6,7]

Acknowledgment. This work was supported by Grant-in-Aid for Science Research from the Ministry of Education, Science, Sports, and Culture of Japan.

References and Notes

(1) Natta, G.; Corradini, P. *Nuovo Cimento (Suppl.)* **1960**, *15*, 40.
(2) Mencik, Z. *J. Macromol. Sci., Phys.* **1972**, *B6*, 101.
(3) Turner-Jones, A.; Aizlewood, J. M.; Beckett, D. R. *Makromol. Chem.* **1964**, *75*, 134.
(4) Lotz, B.; Wittmann, J. C.; Lovinger, A. J. *Polymer* **1996**, *37*, 4979.
(5) See for example: Chu, F.; Yamaoka, T.; Ide, H.; Kimura, Y. *Polymer* **1994**, *35*, 3442.
(6) Alamo, R. G.; Kim, M. H.; Galante, M. J.; Isasi, J. R.; Mandelkern, L. *Macromolecules* **1999**, *32*, 4050.
(7) van der Burgt, F. P. T. J.; Rastogi, S.; Chadwick, J. C.; Rieger, B. *J. Macromol. Sci., Phys.* **2002**, *B41*, 1091.
(8) Assouline, E.; Fulchiron, R.; Gerard, J.-F.; Wachtel, E.; Wagner, H. D.; Marom, G. *J. Polym. Sci., Part B: Polym. Phys.* **1999**, *37*, 2534.
(9) Coccorullo, I.; Pantani, R.; Titomanlio, G. *Polymer* **2003**, *44*, 307.
(10) Hsu, C. C.; Geil, P. H.; Miyaji, H.; Asai, K. *J. Polym. Sci., Polym. Phys.* **1986**, *24*, 2379.
(11) Hosemann, R.; Wilke, W. *Makromol. Chem.* **1968**, *118*, 230.
(12) Miller, R. *Polymer* **1960**, *1*, 135.

(13) Grebowicz, J.; Lau, S.-F.; Wunderlich, B. *J. Polym. Sci., Polym. Symp.* **1984**, *71*, 19.
(14) Caldas, V.; Brown, G. R.; Nohr, R. S.; MacDonald, J. G.; Raboin, L. E. *Polymer* **1994**, *35*, 899.
(15) Ferrero, A.; Ferracini, E.; Mazzavillani, A.; Malta, V. *J. Macromol. Sci., Phys.* **2000**, *B39*, 109.
(16) Lotz, B. *Eur. Phys. J. E* **2000**, *3*, 185.
(17) Ogawa, T.; Miyaji, H.; Asai, K. *J. Phys. Soc. Jpn.* **1985**, *54*, 3668.
(18) Grubb, D. T.; Yoon, D. Y. *Polym. Commun.* **1986**, *27*, 84.
(19) Miyamoto, Y.; Fukao, K.; Yoshida, T.; Tsurutani, N.; Miyaji, H. *J. Phys. Soc. Jpn.* **2000**, *69*, 1735.
(20) Wang, Z. G.; Hsiao, B. S.; Srinivas, S.; Brown, G. M.; Tsou, A. H.; Cheng, S. Z. D.; Stein, R. S. *Polymer* **2001**, *42*, 7561.
(21) Martorana, A.; Piccarolo, S.; Sapoundjieva, D. *Macromol. Chem. Phys.* **1999**, *200*, 531.
(22) Imai, M.; Mori, K.; Mizukami, T.; Kaji, K.; Kanaya, T. *Polymer* **1992**, *33*, 4451.
(23) Imai, M.; Kaji, K.; Kanaya, T. *Phys. Rev. Lett.* **1993**, *71*, 4162.
(24) Imai, M.; Kaji, K.; Kanaya, T. *Macromolecules* **1994**, *27*, 7103.
(25) Matsuba, G.; Kaji, K.; Nishida, K.; Kanaya, T.; Imai, M. *Macromolecules* **1999**, *32*, 8932.
(26) Zemke, K.; Schmidt-Rohr, K.; Spiess, H. W. *Acta Polym.* **1994**, *45*, 148.
(27) Nishida, K.; Konishi, T.; Kanaya, T.; Kaji, K. *Polymer* **2004**, *45*, 1417.
(28) Turner-Jones, A. *Polymer* **1971**, *12*, 487.
(29) Cheng, S. Z. D.; Janimak, J. J.; Zhang, A.; Hsieh, E. T. *Polymer* **1991**, *32*, 648.
(30) Kissin, Y. V. *Adv. Polym. Sci.* **1974**, *15*, 91.
(31) Brandrup, J.; Immergut, E. H.; Grulke, E. A. *Polymer Handbook,* 4th ed.; John Wiley & Sons: New York, 1999.
(32) Kissin, Y. V.; Tsvetkova, V. I.; Chirkov, N. M. *Eur. Polym. J.* **1972**, *8*, 529.
(33) Kissin, Y. V.; Rishina, L. A. *Eur. Polym. J.* **1976**, *12*, 757.
(34) Kobayashi, M.; Akita, K.; Tadokoro, H. *Makromol. Chem.* **1968**, *118*, 324.
(35) Hanna, L. A.; Hendra, P. J.; Maddams, W.; Willis, H. A.; Zichy, V.; Cudby, M. E. A. *Polymer* **1988**, *29*, 1843.
(36) Passingham, C.; Hendra, P. J.; Cudby, M. E. A.; Zichy, V.; Weller, M. *Eur. Polym. J.* **1990**, *26*, 631.
(37) Strobl, G. *The Physics of Polymer*; Springer-Verlag: Berlin, 1997.
(38) Zhu, X.; Yan, D.; Fang, Y. *J. Phys. Chem. B* **2001**, *105*, 12461.
(39) Conformational transition rate constants for molten polypropylenes were estimated by a molecular dynamics (MD) study (Antoniadis, S. J.; Samara, C. T.; Theodorou, D. N. *Macromolecules* **1999**, *32*, 8635). The rate constant of iPP rapidly decays, and it becomes very small (less than 1/10 that of the melt) at 0 °C when the simulated trend is extrapolated exponentially to the lower temperatures. Thus, we assume the 3/1 helices of iPP in the deeply quenched state are stiff.
(40) Doi, M.; Edwards, S. F. *The Theory of Polymer Dynamics*; Oxford: New York, 1986.

MA050908F